UC Davis

UC Davis Previously Published Works

Title

Biaxial Residual Stress Mapping for a Dissimilar Metal Welded Nozzle

Permalink

https://escholarship.org/uc/item/6b0637b8

Journal

Journal of Pressure Vessel Technology, 138(1)

ISSN

0094-9930

Authors

Hill, Michael R
Olson, Mitchell D
DeWald, Adrian T

Publication Date

2016-02-01

DOI

10.1115/1.4031504

Peer reviewed

eScholarship.org Powered by the California Digital Library
University of California

Biaxial Residual Stress Mapping for a Dissimilar Metal Welded Nozzle

Michael R. Hill[1], Mitchell D. Olson[1], and Adrian T. DeWald[2]
[1]University of California, Davis
Department of Mechanical and Aerospace Engineering,
One Shields Avenue, Davis, CA 95616 USA
[2] Hill Engineering, 3035 Prospect Park, Rancho Cordova, CA 95670 USA

Submitted to Journal of Pressure Vessel Technology, October 2014
Revised manuscript submitted June 2015
Revised manuscript accepted August 2015
https://doi.org/10.1115/1.4031504

Abstract

This paper describes a sequence of residual stress measurements made to determine a two-dimensional map of biaxial residual stress in a nozzle mockup having two welds, one a dissimilar metal (DM) weld and the other a stainless steel (SS) weld. The mockup is cylindrical, designed to represent a pressurizer surge nozzle of a nuclear pressurized water reactor (PWR), and was fabricated as part of a weld residual stress measurement and finite element modeling round robin exercise. The mockup has a nickel alloy DM weld joining a SS safe end to a low-alloy steel cylinder and stiffening ring, as well as a SS weld joining the safe end to a section of SS pipe. The biaxial mapping experiments follow an approach described earlier, in PVP2012-78885 and PVP2013-97246, and comprise a series of experimental steps and a computation to determine a two-dimensional map of biaxial (axial and hoop) residual stress near the SS and DM welds. Specifically, the biaxial stresses are a combination of a contour measurement of hoop stress in the cylinder, slitting measurements of axial stress in thin slices removed from the cylinder wall, and a computation that determines the axial stress induced by measured hoop stress. At the DM weld, hoop stress is tensile near the OD (240 MPa) and compressive at the ID (-320 MPa), and axial stress is tensile near the OD (370 MPa) and compressive near the mid-thickness (-230 MPa) and ID (-250 MPa). At the SS weld, hoop stress is tensile near the OD (330 MPa) and compressive near the ID (-210 MPa), and axial stress is tensile at the OD (220 MPa) and compressive near mid-thickness (-225 MPa) and ID (-30 MPa). The measured stresses are found to be consistent with earlier work in similar configurations.

Introduction

Residual stresses are known to contribute to crack growth in metals, with tensile residual stress increasing crack growth rates and compressive residual stress decreasing crack growth rates [1]. In many cases, highly tensile residual stress has been found in welds [2], often on the order of the yield strength [3]. The piping system in nuclear power plants is typically welded together, as is the case in the primary reactor piping, where both axial and circumferential cracks can possibly develop over time [4, 5]. In welded piping systems of pressurized water reactors (PWRs), primary water stress corrosion cracking is an important crack driving mechanism [6], where weld residual stress is a key parameter. Thus, it is important to understand the state of residual stress in piping welds, where both axial and hoop (circumferential) stresses may drive cracks.

Near a cylindrical welded joint, axial and hoop stresses vary in both the radial and axial directions. They may also vary in the circumferential direction, but the stresses are frequently assumed to have axial symmetry [7]. Computational finite element weld models have been used to understand the two-dimensional variation of stress in welded joints, and the output of such models used to support flaw assessment and plant management decisions. Biaxial maps of measured residual stress should be useful for validation of weld models, providing two-dimensional maps of the axial and hoop stresses that support flaw assessment procedures. However, recent work shows difficulty in making residual stress measurements in prototypic PWR welds [8, 9], and although there are many different residual stress measurement techniques available (each measuring limited spatial range and limited stress components) [10], recent work by the authors has developed a new method for biaxial stress mapping in welded cylinders [11, 12].

Here we report on measurements made in the context of weld residual stress model validation, performed on a mockup nozzle from the cooperative program on welding residual stress (WRS) organized by the Electric Power Research Institute (EPRI) and the United States Nuclear Regulatory Commission (NRC). Results of previous phases of this program can be found in [13, 14]. The WRS program has worked to systematically validate computational weld models in a series of mockups of increasing complexity [15]. The measurements in this paper were performed on the Phase 2a mockup [16], which represents a prototypic cylindrical nozzle with two welds, a dissimilar metal (DM) weld and a stainless steel (SS) weld.

The measurements provide maps of the axial and hoop stress along a radial-axial plane of interest, in the region of the two welds. The methods follow the approach developed in [11] and [12], and comprise a combination of sectioning (with strain gages), a contour measurement to determine hoop stress, slitting measurements to determine axial stress in thin slices removed from the cylinder wall, and a computation that determines the axial stress induced by measured hoop stress. It is assumed that sectioning causes elastic stress release and that the stress state near the radial-axial plane of interest is locally axisymmetric. The measurement steps were designed to provide the highest possible measurement fidelity for the approach used and the uncertainty of the method [17] has been found to be in line with the precision of the contour method [18].

Methods

Measurements were performed on a prototypic mockup representing a PWR pressurizer safety and relief nozzle, identified as the Phase 2a nozzle in the EPRI/NRC program on welding residual stresses. The mockup is an idealized nuclear power plant nozzle that would attach SS piping (right side of Fig. 1a) to a pressure vessel (left side of Fig. 1a) using a “safe end”. The pressure vessel side of the mockup is carbon steel (SA-105) and the piping side, safe end, and cladding are stainless steel (316 SS) (Fig. 2a). The weld attaching the pressure vessel to the safe end consists of a buttering layer and weld, both made of nickel-based weld metal (Alloy 82). Connecting the safe end to the SS piping is a SS weld made of 316 stainless steel. The material elastic properties are given in Table 1.

The nozzle mockup is 790 mm (31.1 in) long, with a 284.5 mm (11.2 in) inner diameter (Fig. 1a). The nozzle wall had a variable thickness that was 48.25 mm (1.9 in) on the pressure vessel side and 36.25 mm (1.4 in) on the SS piping side (Fig. 1a). For convenience, local coordinate systems for each weld will be used throughout this paper, where each local origin is at the center of the weld (either the DM or SS weld) at the ID with the positive x-axis toward the SS piping and the positive r-axis toward the OD (Fig. 2b, showing a global coordinate system).

To find the axial and hoop stress at a specified plane of interest in the nozzle (dashed plane in Fig. 3), several experimental steps with superposition will be used, as shown in Fig. 3. Each experimental step will remove material from the part and will change its configuration, where each configuration will be identified by a capital letter (e.g., A). The experiments involve four configurations: original configuration (A), after sectioning (B), after contour cut (C), and after removing a thin slice (D).

The stress in each configuration, at the plane of interest, will be identified with a superscript (e.g., stress in configuration A is denoted σ^A (all components of the stress tensor)), and during the experiments, there is a change of stress attending each change of configuration. Residual stress released between the current configuration and the prior configuration is identified with an italic roman numeral (e.g., $\sigma^i = \sigma^A - \sigma^B$). Fig. 3 shows all configuration changes and their associated stress release. With superposition, σ^A can be found as

$$\sigma^A = \sigma^i + \sigma^{ii} + \sigma^{iii} + \sigma^D. \quad (1)$$

A fundamental challenge in these measurements is to robustly quantify stress release attending each configuration change using the principles of elastic mechanical stress release methods.

The change between configurations A and B occurs in five sectioning steps. The first two steps removed the ends of the mockup, by cutting 139.7 mm (5.5 in) and 463.55 mm (18.25 in) from the mockup base, as shown by the red dashed lines in Fig. 1a. In the next step, a band saw was used to cut a radial slot into the nozzle at a clock position of 60º (Fig. 4). The purpose of this cut was to release the through wall bending moment, which reduced the possibility for yielding in subsequent steps. The final two steps isolated configuration B with band saw cuts at 240º and 345º, providing a small section suitable for further work.

Stress release from configuration A to B was found by combining elastic stress analysis with strain measured near the plane of interest. Before sectioning, biaxial (hoop and axial) strain gage rosettes were applied to the nozzle OD and ID at the plane of interest (clock position of 292.5º) at the center of the DM weld and at ±25.4 mm from the center of the DM weld. Strain changes were measured for each of the sectioning steps, and elastic finite element analysis was used to relate a normal traction field at the cut plane to strain at the set of gage locations. The finite element analysis used linear displacement interpolation elements and included the different materials present in the nozzle. For cuts along a radial-axial plane (shown in Fig. 4), the cut plane traction (acting in the hoop direction) was assumed to be bilinear in the cut plane, having three unknown coefficients. For cuts along a radial-hoop plane (shown as red dashed lines in Fig. 1a), the cut plane traction (acting in the axial direction) was assumed to be linear with radial position, and axisymmetric, having two unknown coefficients. For each cut, unknown coefficients were determined from measured strain data using least squares, and the traction fields then provide stress release from A to B (σ^i). The simple linear or bilinear traction fields are suitable for the A to B sectioning steps because the sectioning planes are remote from the section of interest, and the major sources of stress release are the effects of axial and hoop direction section forces (largely bending moments).

The stress release between configurations B and C, σ^{ii}, is found using the contour method, which determines both the axial and hoop stress change on the plane of interest. The contour measurement is detailed in a companion paper [19], followed typical procedures [20], and is summarized here. The first step of the contour measurement cuts the nozzle section in half at the plane of interest using wire electric discharge machining (EDM). Subsequent steps measure the out-of-plane profile of cut surface on both halves of the part, fit each profile to a smoothing analytical surface, and average the two profiles on a

common grid of points on the cut plane. The average profile is then used as a set of displacement boundary conditions on the cut face of a linear elastic finite element model of half the part, which provides residual stress change on the cut plane. The total hoop stress in configuration A can now be found by superposing the released hoop stress from sectioning (σ^{i}) and the contour measurement (σ^{ii}), because subsequent configuration changes do not affect the hoop stress at the plane of interest.

The change between configurations C and D is due to removing a thin slice from the mockup. The stress release from removing a thin slice, σ^{iii}, is difficult to obtain through experiment. Earlier work shows that this measurement can be avoided by decomposing stress in configuration B into the stress remaining in the removed slice (σ^{D}) and the stress in D caused by the out-of-plane component of σ^{B}, as illustrated in Fig. 5. A numerical validation [17] has shown this stress decomposition to be valid. The stress decomposition can be expressed as

$$\sigma^{B} = \sigma^{B(\theta)} + \sigma^{D} \tag{2}$$

where $\sigma^{B(\theta)}$ is the effect of the hoop stress on a thin slice. To determine $\sigma^{B(\theta)}$, only the hoop stress that was determined from σ^{ii} is required, which allows σ^{B} to be determined without directly measuring σ^{iii}. The same principle applies to the original configuration, i.e. $\sigma^{A} = \sigma^{A(\theta)} + \sigma^{D}$, but since the part is undergoing several non-symmetric sectioning cuts it is convenient to apply the stress decomposition to σ^{B}. The original stress can then be found as

$$\sigma^{A} = \sigma^{i} + \sigma^{B} = \sigma^{i} + \sigma^{B(\theta)} + \sigma^{D}. \tag{3}$$

The stress $\sigma^{B(\theta)}$ was found with a linear elastic stress analysis using commercial finite element software package [21]. The stress analysis consisted of applying the hoop stress from the contour measurement (σ^{ii}) as a traction boundary condition on the faces of a thin slice, and extracting the (in-plane) axial stress at equilibrium. The thin slice was 5 mm thick (same geometry as the slices used to determine σ^{D} as will discussed shortly). The model had a mesh with node spacing of 1 mm by 1 mm in the in-plane directions and eight elements across the thickness, with a total of roughly 150,000 reduced integration eight node linear brick elements (C3D8R). The material was assumed to be linear elastic with a Young's modulus of 207 GPa and Poisson's ratio of 0.28, since there is little variation in elastic material properties over the cross-section. Only half of the slice was modeled to save computational time by using a symmetry boundary condition at the slice mid-thickness

Three slices of configuration D were removed from configuration C. Each slice was cut on a radial-axial plane with a thickness of 5 mm at the mid-wall, and slightly thicker near the OD and thinner near the ID. Axial stress remaining in each slice (σ^{D}) was found with multiple slitting measurements to develop a map of axial stress. Slitting determines axial stress by the incremental cutting of a thin slit in the radial direction (releasing the axial stress) starting at the ID and measuring strain at the back face (OD) after each cut increment. Near the DM weld, slitting measurements were spaced 20 mm apart and in the SS weld, they were 15 mm apart. Two of the slices (slices 1 and 3) had identical measurement locations, with one slit at the weld center, and the remaining slice (slice 2) had measurement locations mid-way between (Fig. 2b). It is assumed that stresses are locally axisymmetric near the plane of interest, so that the measurements in different slices reflected stresses at the plane of interest. Slitting measurements were preformed according to typical procedures, consisting of cutting along the radial direction in small increments of depth with wire EDM while measuring strain as a function of slit depth at the back face of the slit plane. Stress as a function of position is then calculated from strain versus slit depth data using an elastic inverse and Tikhonov regularization. Methodological details can be found in

[22] and [23]. The uncertainty associated with the slitting measurements was estimated using the procedure given in [24]. Since regularized unit pulses were used as the basis functions, the model error term in [24] was excluded and the random uncertainty term was taken as the maximum of either the misfit between measured strain and fit strain, or a minimum value of 2 με. The reported values of the measured axial stress with slitting are the average of the two measured stresses in slices 1 and 3 and the reported uncertainty is the uncertainty of the mean, which for two measurements is half of the root sum square of the uncertainties measured in each slice. Since multiple slitting measurements were performed on each slice, the stress change at the current measurement location caused by a previous measurement is needed and is found with a supplemental stress analysis. The analysis consists of applying the previously measured stress to a finite element model of the part and extracting the resulting stress at the future measurement location, as was shown in [25, 26].

Results

All the hoop and axial stress measurements around the DM weld can be seen in Fig. 6. The hoop stress release from sectioning (Fig. 6a) reflects through-wall bending with a minimum of -65 MPa at the ID and a maximum of 110 MPa at the OD. The hoop stress results from the contour measurement (Fig. 6b) show tensile stresses near the OD with a maximum in the weld at 150 MPa and compressive stress along the ID with a minimum in the cladding at -220 MPa. The total hoop stress (Fig. 6d) is tensile near the OD with a maximum of 240 MPa and compressive along the ID with a minimum in the cladding at -320 MPa. The axial stress release from sectioning (Fig. 6a) reflects through-wall bending with a minimum of -110 MPa at the ID and a maximum of 110 MPa at the OD. The effect of the hoop stress on the slice (Fig. 6b) resembles a through-wall bending stress distribution, with tensile stress at the OD (maximum near 330 MPa) and compressive stress at the ID (minimum near -320 MPa). The axial stress in the slice (Fig. 6c) measured with slitting has a banded structure with tensile stresses at the ID and OD (maximum near 145 MPa) and compressive stress at the mid-thickness (minimum near -200 MPa). The total axial stress (Fig. 6d) has a banded structure, alternating between compression at the ID and tension near the OD. The maximum is near the OD in the weld at 370 MPa and the minimum around the mid-thickness in the weld at -230 MPa. Line plots of each contributor to the axial stress at the center of the DM weld can be seen in Fig. 7a. The results show that both the stresses in the slice and the effect from the hoop stress are significant contributors to the total.

All the hoop and axial stress measurements around the SS weld can be seen in Fig. 8. The hoop stress release from sectioning (Fig. 8a) reflects through-wall bending with a minimum of -50 MPa at the ID and a maximum of 75 MPa at the OD. The hoop stress results from the contour measurement (Fig. 8b) show tensile stresses near the OD with a maximum of 230 MPa and compressive stress near the ID with a minimum at -170 MPa. The total hoop stress (Fig. 8d) is tensile near the OD, with a maximum of 330 MPa, and compressive near the ID, with a minimum at -210 MPa. The axial stress release from sectioning (Fig. 8a) reflects through-wall bending and is small with a minimum of -10 MPa at the ID and a maximum of 10 MPa at the OD. The effect of the hoop stress on the slice (Fig. 8b) resembles a through-wall bending distribution, with tensile stress at the OD (maximum around 45 MPa) and compressive stress at the ID (minimum around -150 MPa). The axial stress in the slice (Fig. 8c) measured with slitting has a banded structure with tensile stresses at the ID and OD (maximum around 190 MPa) and compressive stress at the mid-thickness (minimum around -170 MPa). The total axial stress (Fig. 8d) alternates between tension at the OD and compression at the ID. The maximum stress is 250 MPa and occurs at about 30 mm from the bottom of the ID, and the minimum stress is -225 MPa and occurs near mid-wall, at the weld/pipe interface. Line plots of the axial stress at the center of the SS weld can be seen in Fig. 7b. The results confirm what was seen in the DM weld; stress in the slice and the effect of hoop stress each contribute significantly to the total.

The uncertainty in axial stress from slitting can be found in Fig. 9 for both the DM and SS welds. The results show the uncertainties are significantly higher for the DM weld with a maximum of 20 MPa. The uncertainty is consistently larger near the initial slitting cut depths, which is expected because strain measurements are the least sensitive to stress release at these locations. The uncertainties in the SS weld are significantly lower than what was found in the DM weld, with a maximum of 6 MPa, but show the same trend with uncertainty highest at the initial cuts of the slitting measurement.

Discussion

The EPRI/NRC WRS program included a round-robin modeling activity, where a number of research teams submitted weld model results blind to measurement data. Model outputs submitted in the round robin were described earlier [14], and a comparison between model results and measured stresses at the center of the DM weld is shown in Fig. 10. Each round robin participant choose several key modeling parameters and inputs, notably the participants used a wide range of constitutive relations. Thin lines in Fig. 10 show each participant submission, while dark lines show the average of all model output submissions and available experimental data. Experimental data in Fig. 10 include the present work, axial stress from a contour measurement (unique from the axial measurements presented earlier) [19], and results of deep hole drilling (DHD) [14]. Overall, the comparison between the present method and DHD is reasonable, with good agreement in the hoop stress over most of the thickness (somewhat large differences toward the OD) and limited agreement in the axial stress (current method measures somewhat lower stresses toward the ID and OD than DHD). Despite the large spread in model outputs, there is a level of agreement between the measurement data and model average.

Despite the complexity in experimental methods, the present work provides stresses that are in reasonable agreement with weld model outputs and other experimental data. Broussard et al. [27] performed a welding simulation for this nozzle using a commercial finite element software [28]. They used decoupled thermal and mechanical analyses, the latter using an elastic, perfectly-plastic constitutive (stress-strain) relation. The predicted residual stresses in the DM weld are given in Fig. 6e. The measurement data and model output for hoop stress show significant differences in magnitude, but have similar spatial features, both showing tensile stress near the OD and ID and low magnitude stresses at the mid-thickness. For the axial stress, the measurement data and model output have striking agreement. A likely cause of the significant difference in hoop stress magnitude is the simplistic constitutive relation used in the weld model.

The model output and measurement data for residual stress in the SS weld can be compared in Fig. 8e. The trends in measurement-model comparison noted for the DM weld apply equally to the SS weld. The spatial distribution of the hoop stress is in reasonable agreement, but there is a significant difference in magnitude, and there is striking agreement for the axial stress.

Since repeat measurement data for slitting are available, it is interesting to determine the level of measurement repeatability. The two slitting measurements at the center of the DM weld in slices 1 and 3 can be seen in Fig. 11a. The measured stresses in each slice are similar overall, with some areas of notable difference. Toward the ID, the measured stresses differ by roughly 40 MPa, but the uncertainty in each measurement (error bar in Fig. 11a) near the ID is similar to the 40 MPa difference. Near the OD, the measured stresses differ by about 30 MPa, and the uncertainty in this region is smaller. Plotting the absolute value of the difference between the measurements, called the range, along with the combined uncertainty of the two measurements (root sum square of the two uncertainties), as a function of radial position (Fig. 11b), shows that measured stresses in the two slices are, overall, statistically different. Although the stresses in the two slices differ, the differences are small (about 30 MPa) relative to the level of total axial stress in the nozzle (peak of about 370 MPa).

Summary

This paper presents results of biaxial residual stress mapping in the Phase 2a nozzle mockup from the EPRI/NRC program on welding residual stress. The hoop stress was used as an input for the biaxial mapping, which determined axial stresses remaining in thin slices and the effect of hoop stress on the axial stress, following the recently developed approach described earlier [11, 12].

The hoop residual stress in the DM weld is tensile along the OD with a maximum of 240 MPa near the last weld bead, and is compressive along the ID with a minimum of -320 MPa in the cladding. The axial stress in the DM weld has a banded structure, alternating between compression at the ID, tension around the quarter thickness, compression around the mid-thickness, and back to tension at the OD with the maximum of 370 MPa near the OD and minimum of -230 MPa in the weld, near the mid-thickness. The measured stresses were found to have reasonable agreement with measurement and modeling results for the same mockup that had been published earlier.

Acknowledgements

The Electric Power Research Institute, Materials Reliability Program (Paul Crooker, Principal Technical Leader) provided financial support for the axial stress mapping measurements presented here. The U.S. NRC commissioned the hoop measurements from Hill Engineering, LLC that are reported here. We acknowledge John Broussard (Dominion Engineering, Inc.) for help regarding computational weld modeling and for modeling results.

References

[1] D. H. Stuart, "Evaluation of Linear Elastic Fracture Mechanics Predictions of One and Two-Dimensional Fatigue Crack Growth at Cold-Expanded Holes", Masters of Science, Mechanical and Aerospace Engineering, University of California, Davis, 2010.

[2] O. Muránsky, M. C. Smith, P. J. Bendeich, T. M. Holden, V. Luzin, R. V. Martins*, et al.*, "Comprehensive numerical analysis of a three-pass bead-in-slot weld and its critical validation using neutron and synchrotron diffraction residual stress measurements", *International Journal of Solids and Structures,* vol. 49, pp. 1045-1062, 2012.

[3] L. F. Fredette, J. E. Broussard, M. Kerr, and H. J. Rathbun, "NRC/EPRI Welding Residual Stress Validation Program - Phase III Details and Findings", PVP2011-57645, ASME 2011 Pressure Vessels & Piping Division Conference, Baltimore, MD, USA, 2011.

[4] A. R. McIlre, "PWR Materials Reliability Project Interim Alloy 600 Safety Assessments for US PWR Plants (MRP-44)- Part 1: Alloy 82/182 Pipe Butt Welds", Electric Power Research Institute, Palo Alto, CA, 2001.

[5] W. Bamford, B. Newton, and D. Seeger, "Recent experience with weld overlay repair of indications in alloy 182 butt welds in two operating PWRs", PVP2006-ICPVT-11-93891, ASME 2006 Pressure Vessels and Piping/ICPVT-11 Conference, 2006.

[6] J. Hickling, "Material Reliability Program Crack Growth Rates for Evaluating Primary Water Stress Corrosion Cracking (PWSCC) of Alloy 82, 182, and 132 Welds", MRP-115NP, Electric Power Research Institute, Palo Alto, CA,, 2004.

[7] O. Muránsky, M. C. Smith, P. J. Bendeich, and L. Edwards, "Validated numerical analysis of residual stresses in Safety Relief Valve (SRV) nozzle mock-ups", *Computational Materials Science,* vol. 50, pp. 2203-2215, 2011.

[8] P. J. Withers, M. Turski, L. Edwards, P. J. Bouchard, and D. J. Buttle, "Recent advances in residual stress measurement", *International Journal of Pressure Vessels and Piping,* vol. 85, pp. 118-127, 2008.

[9] W. Woo, G. B. An, E. J. Kingston, A. T. DeWald, D. J. Smith, and M. R. Hill, "Through-thickness distributions of residual stresses in two extreme heat-input thick welds: A neutron diffraction, contour method and deep hole drilling study", *Acta Materialia,* vol. 61, pp. 3564-3574, 2013.

[10] G. S. Schajer and C. O. Ruud, Ch. 1: Overview of Residual Stresses and Their Measurement in *Practical Residual Stress Measurement Methods*, Ed. G. S. Schajer, John Wiley & Sons, West Sussex, UK, 2013

[11] M. R. Hill and M. D. Olson, "Biaxial Residual Stress Mapping in a PWR Dissimilar Metal Weld", PVP2013-97246, ASME 2013 Pressure Vessels & Piping Division Conference, Paris, France, 2013.

[12] M. D. Olson, W. Wong, and M. R. Hill, "Simulation of Triaxial Residual Stress Mapping for a Hollow Cylinder", PVP2012-78885, ASME 2012 Pressure Vessels & Piping Conference, Toronto, Ontario, Canada, 2012.

[13] P. Crooker, "Materials Reliability Program: Finite-Element Model Validation for Dissimilar Metal Butt-Welds", MRP-316, Electric Power Research Institute, Palo Alto, CA, 2011.

[14] H. J. Rathbun, L. F. Fredette, P. M. Scott, A. A. Csontos, and D. L. Rudland, "NRC Welding Residual Stress Validation Program International Round Robin Program and Findings", PVP2011-57642, 2011 ASME Pressure Vessels & Piping Division Conference, Baltimore, MD, USA, 2011.

[15] P. Crooker and A. Csontos, "Cooperative Dissimilar Metal Butt-Weld Residual Stress Finite-Element Model Validation", 2010 Residual Stress Summit, Lake Tahoe, CA, USA, 2010.

[16] M. Kerr and H. J. Rathbun, "Summary of Finite Element (FE) Sensitivity Studies Conducted in Support of the NRC/EPRI Welding Residual Stress (WRS) Program", PVP2012-78883, in *ASME 2012 Pressure Vessels & Piping Division Conference*, Toronto, Ontario, Canada, 2012.

[17] M. D. Olson and M. R. Hill, "A New Mechanical Method for Biaxial Residual Stress Mapping", *Experimental Mechanics,* vol. 55, pp. 1139-1150, 2015.

[18] M. R. Hill and M. D. Olson, "Repeatability of the Contour Method for Residual Stress Measurement", *Experimental Mechanics,* vol. 54, pp. 1269-1277, 2014.

[19] A. T. DeWald, "Measurement of residual stress in reactor mockups containing dissimilar metal welds", PVP2014-28209, ASME 2014 Pressure Vessels & Piping Division Conference, Anaheim, CA, USA, 2014.

[20] M. B. Prime, "Cross-Sectional Mapping of Residual Stresses by Measuring the Surface Contour after a Cut", *Journal of Engineering Materials and Technology,* vol. 123, pp. 162-168, 2001.

[21] Abaqus/Standard, Version 6.10, Providence, RI, USA, 2010.

[22] M. R. Hill, Ch. 4: The Slitting Method in *Practical Residual Stress Measurement Methods*, Ed. G. S. Schajer, John Wiley & Sons, West Sussex, UK, 2013

[23] G. S. Schajer and M. B. Prime, "Use of Inverse Solutions for Residual Stress Measurement", *Journal of Engineering Materials and Technology,* vol. 128, pp. 375-382, 2006.

[24] M. B. Prime and M. R. Hill, "Uncertainty, Model Error, and Order Selection for Series-Expanded, Residual-Stress Inverse Solutions", *Journal of Engineering Materials and Technology,* vol. 128, pp. 175-185, 2006.

[25] W. Wong, "Residual Stress Superposition and the Design and Testing of Coupons for Residual Stress Driven Stress Corrosion Testing", Masters, Mechanical and Aerospace Engineering, University of California, Davis, 2010.

[26] M. D. Olson and M. R. Hill, "Residual Stress Mapping with Slitting", *Manuscript in preparation for publication in Experimental Mechanics,* 2014.
[27] J. E. Broussard, Personal Correspondence, 2014.
[28] ANSYS, Release 13, Canonsburg, PA, USA, 2010.

Tables

Material	E (GPa)	ν	Yield strength (MPa)
Stainless steel alloy 316	207	0.28	560
Carbon steel alloy SA-105	210	0.28	250
Nickel alloy 82/182	214	0.29	410

Table 1: Material properties

Figures

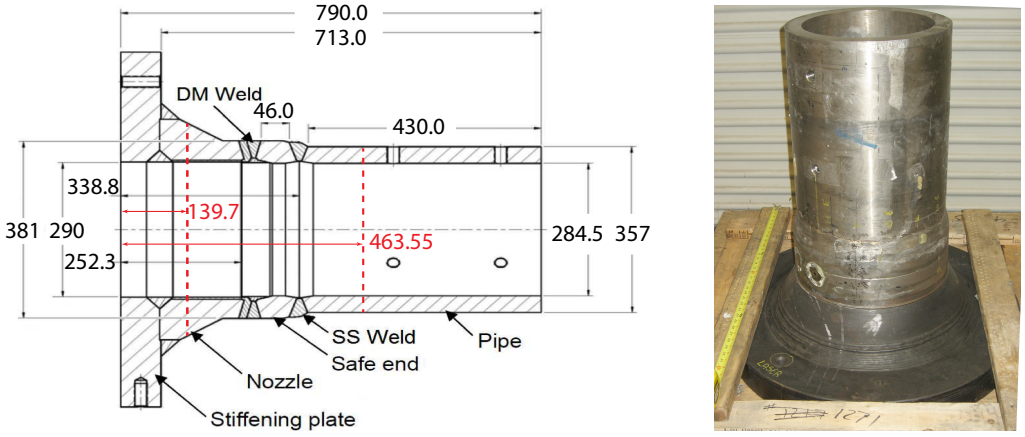

(a) (b)

Fig. 1 – (a) Dimensions of the nozzle mockup (red dashed lines indicate axial sectioning cuts, plane of interest is between the red dashed lines) and (b) photo of its original configuration before sectioning. Dimensions are in mm

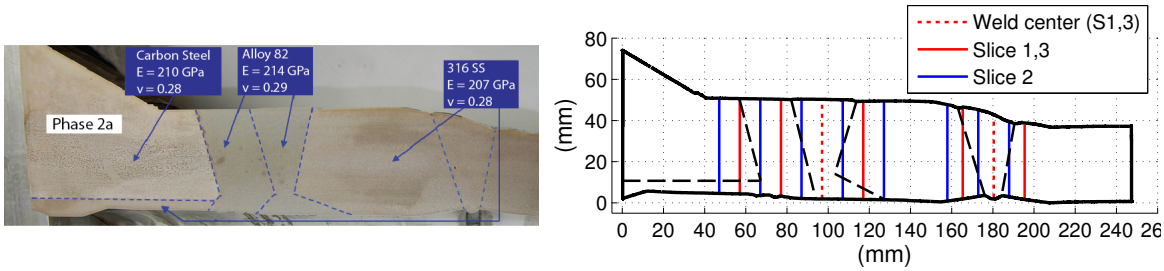

(a) (b)

Fig. 2 – (a) Materials and properties and (b) slitting measurement locations (each colored line is a single slitting measurement)

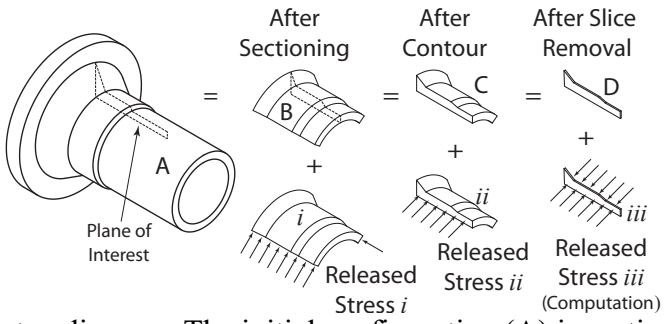

Fig. 3 – Experimental step diagram. The initial configuration (A) is sectioned to the B configuration and the stress release σ^{i} is found with the strain measurements and a finite element calculation. Configuration B is cut in half to configuration C and the stress release σ^{ii} is found with the contour method. A slice (configuration D) is then removed from configuration C. The stress release σ^{iii} is not directly found, but could be found as $\sigma^{iii} = \sigma^{B(\theta)} - \sigma^{ii}$

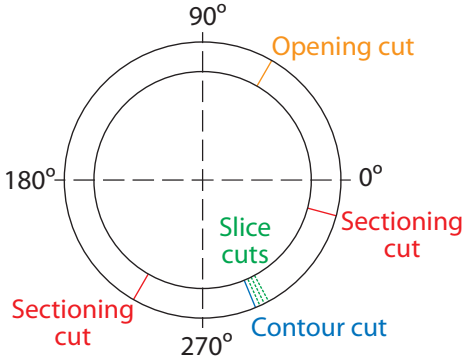

Fig. 4 – Diagram of cut planes. The opening cut is at 60º, the two sectioning cuts are at 240º and 345º, the contour cut is at 292.5º, and the slice cuts are at approximately 295º, 297.5º, and 300º

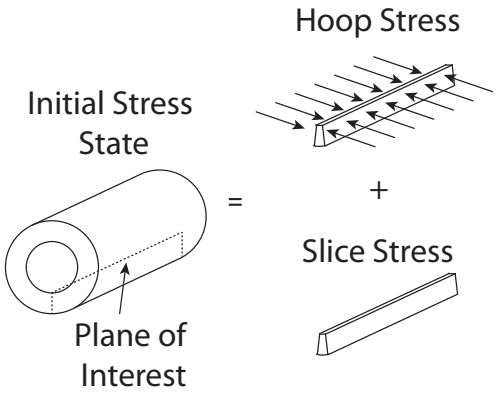

Fig. 5 – Stress decomposition diagram; total stress is a sum of stress in a thin slice and the effect of hoop stress

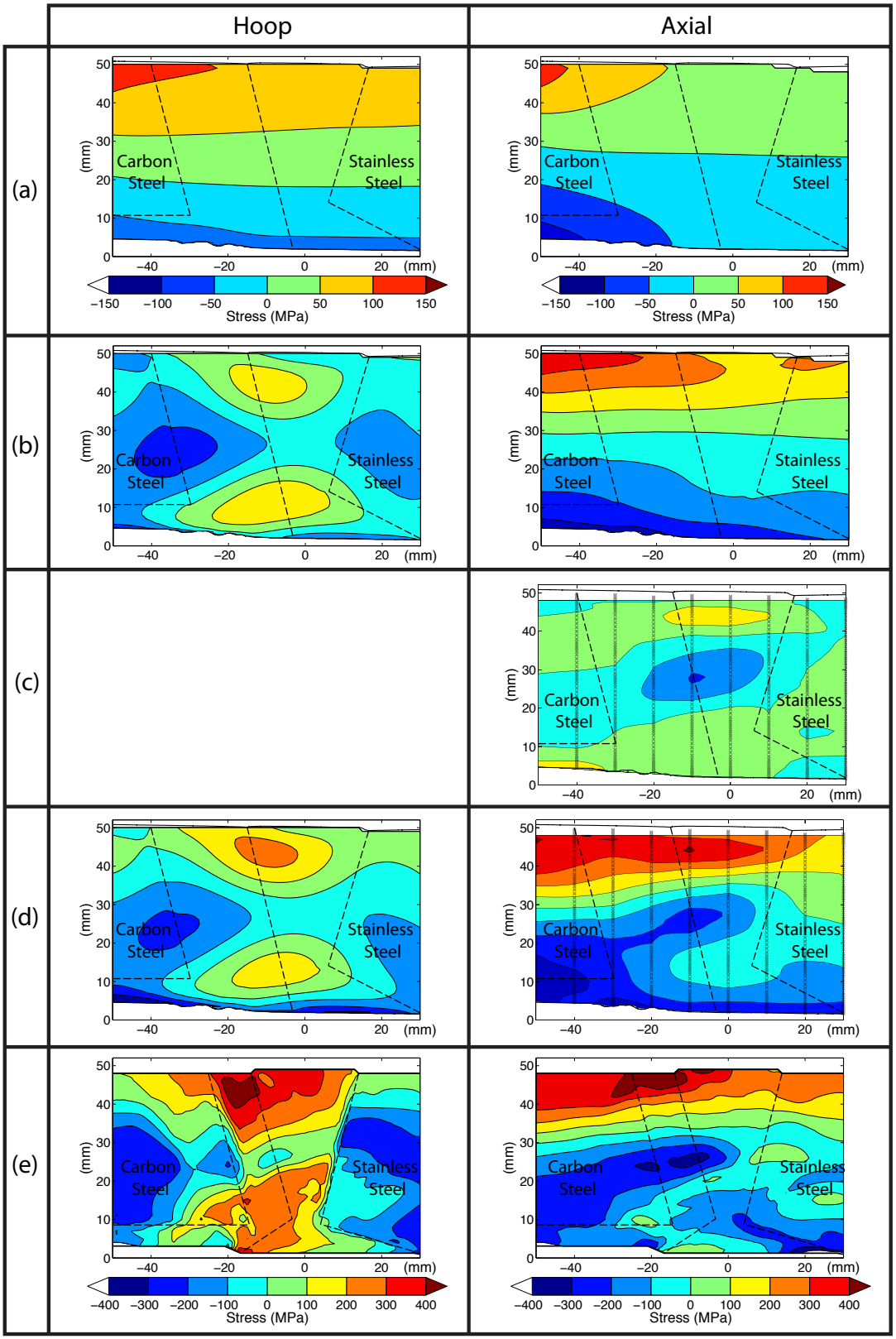

Fig. 6 – DM weld hoop (left) and axial (right) stress (a) release due to sectioning, (b) $\sigma^{B(\theta)}$ (same as contour for hoop stress), (c) slice stress, (d) total residual stress, and (e) FE weld model output from [27]

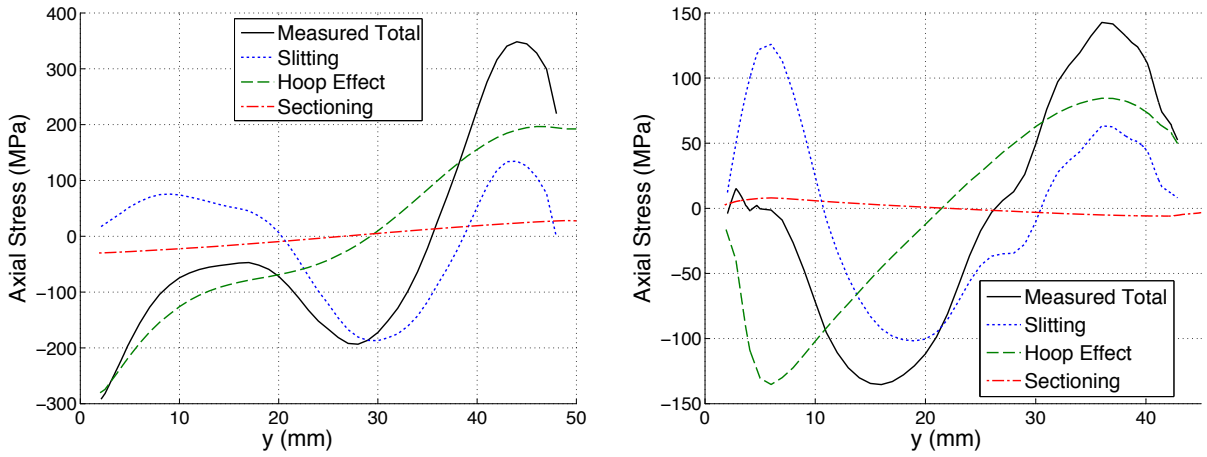

(a) (b)

Fig. 7 – Line plot showing contributions to axial stress at the weld center for (a) DM weld, and (b) SS weld along the radial direction from ID to OD

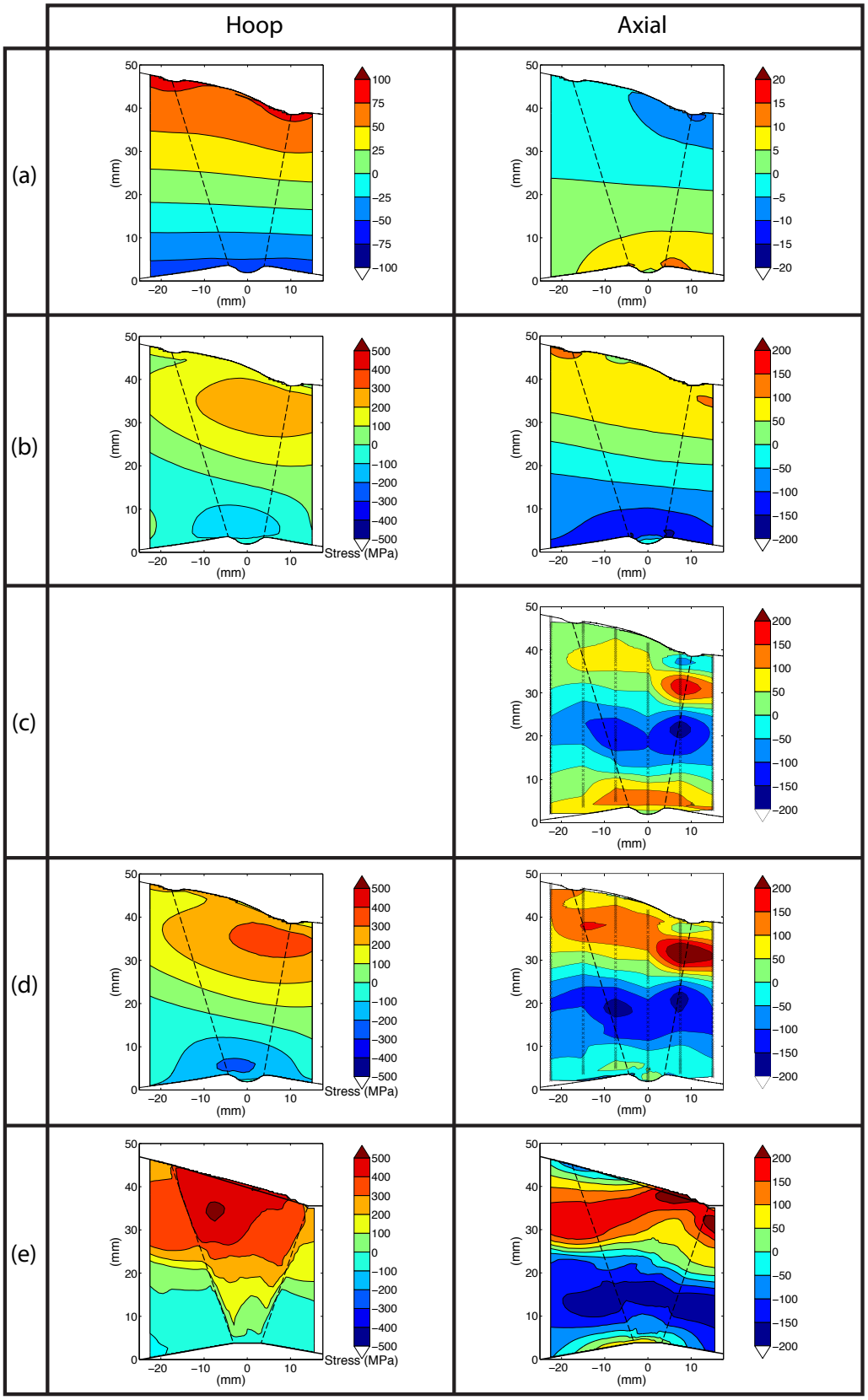

Fig. 8 – SS weld hoop (left) and axial (right) stress (a) release due to sectioning, (b) $\sigma^{B(\theta)}$ (same as contour for hoop stress), (c) slice stress, (d) total residual stress, and (e) FE weld model output from [27]

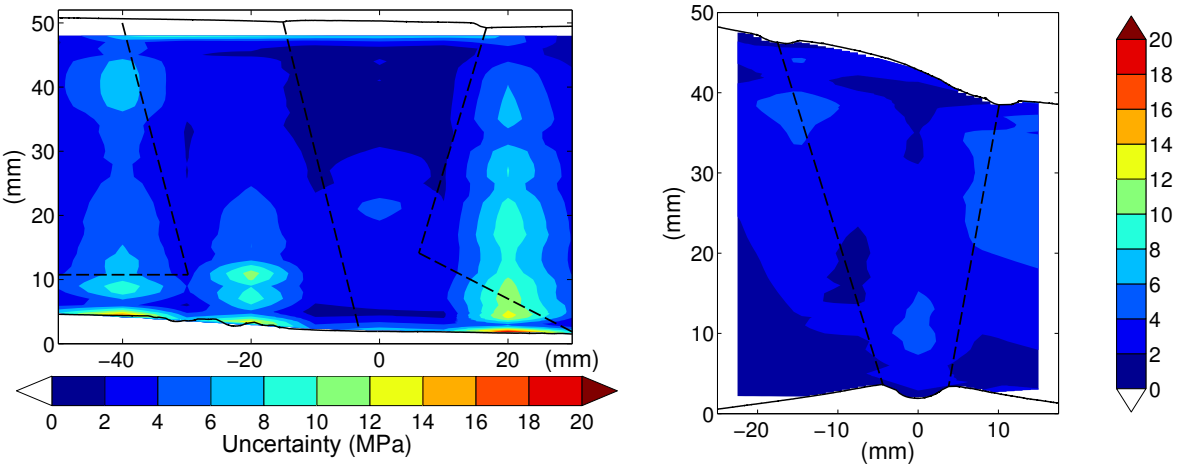

(a) (b)

Fig. 9 – Axial stress uncertainty (95% confidence interval) contour plots for (a) DM weld and (b) SS weld

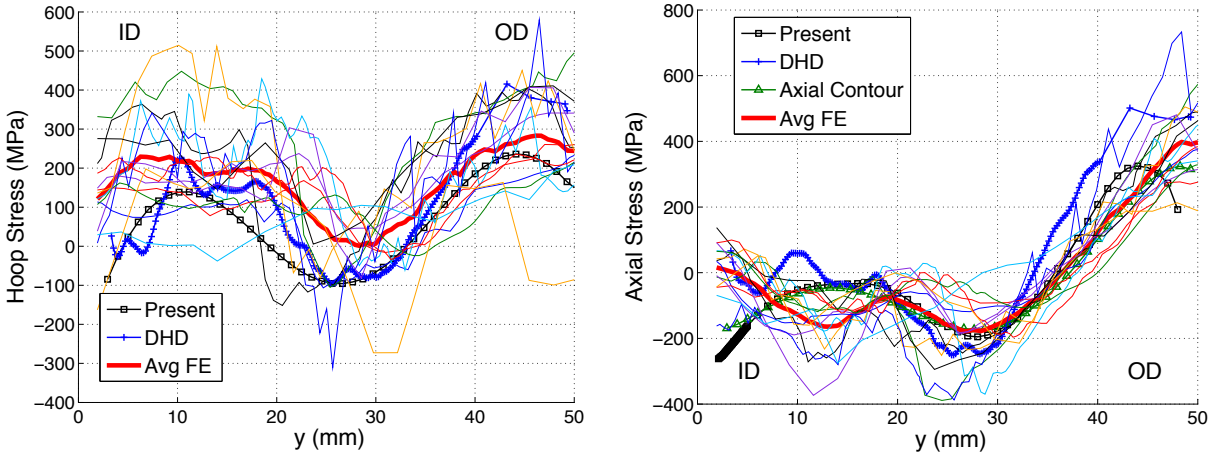

(a) (b)

Fig. 10 – Stress versus through wall position at the center of the DM weld, comparing measurement results with FE model outputs (a) hoop and (b) axial stress

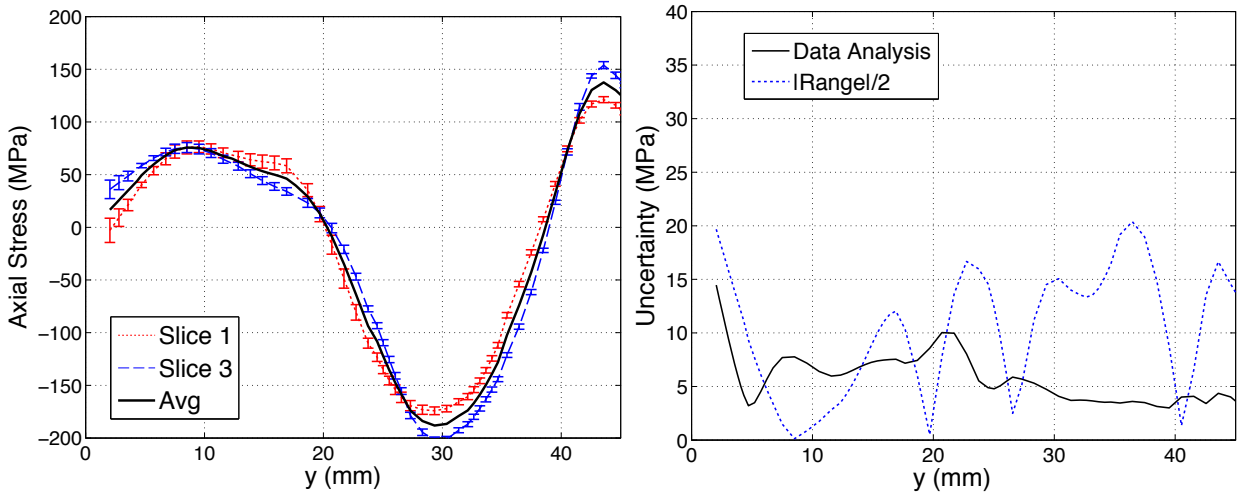

(a) (b)

Fig. 11 – (a) Axial stress results from slitting from slices 1, 3 and (b) combined uncertainty from the root sum square of the two uncertainty estimates calculated in slitting data analysis and half the range of the two measured stresses